Journal of Orthopaedic Translation 52 (2025) 249–264

Contents lists available at ScienceDirect

Journal of Orthopaedic Translation

journal homepage: www.journals.elsevier.com/journal-of-orthopaedic-translation

Review Article

Neuromuscular electrical stimulation alleviates stroke-related sarcopenia by promoting satellite cells myogenic differentiation via AMPK-ULK1-Autophagy axis

Xingdong Xiang [a,1], Lei Huang [b,1], Wenchen Luo [c,1], Lieyang Qin [d], Mengxuan Bian [b], Weisin Chen [b], Guanjie Han [b], Ning Wang [b], Guokang Mo [b], Cheng Zhang [b], Yongxing Zhang [b], Huilin Yang [e], Shunyi Lu [e,*], Jian Zhang [a,**], Tengfei Fu [a,***]

[a] Department of Rehabilitation Medicine, Zhongshan Hospital Fudan University, Shanghai, 200032, China
[b] Department of Orthopedic Surgery, Tongji Hospital, Tongji University School of Medicine, Shanghai, 200065, China
[c] Department of Anesthesiology, Zhongshan Hospital Fudan University, Shanghai, 200032, China
[d] Department of Cardiovascular Surgery, Zhongshan Hospital Fudan University, Shanghai, 200032, China
[e] Department of Orthopedic Surgery, The First Affiliated Hospital of Soochow University, Suzhou, 215123, China

ARTICLE INFO

Keywords:
Stroke-related sarcopenia
Autophagy
Myogenic differentiation
Neuromuscular electrical stimulation
Satellite cells

ABSTRACT

Background: Stroke-related sarcopenia can result in muscle mass loss and muscle fibers abnormality, significantly affecting muscle function. The clinical management of stroke-related sarcopenia still requires further research and investigation. This study aims to explore a promising therapy to restore muscle function and promote muscle regeneration in stroke-related sarcopenia, providing a new theory for stroke-related sarcopenia treatment.

Methods: Stroke-related sarcopenia rat model was established by using permanent middle cerebral artery occlusion (pMCAO) rat and treated with neuromuscular electrical stimulation (NMES). Electrical stimulation (ES) treatment *in vitro* was mimicked to test the effect of NMES on muscle regeneration in rat skeletal muscle satellite cells (MuSCs). Catwalk, H&E and Masson's trichrome staining, immunofluorescence, transcriptomic analysis, transmission electron microscopy, MuSCs transfection, autophagy flux detection, quantitative real-time PCR analysis, Co-Immunoprecipitation and Western Blot were used to investigate the role of NMES and its mechanism in stroke-related sarcopenia *in vivo*.

Results: After NMES treatment, muscle mass and myogenic differentiation were significantly increased in stroke-related sarcopenia rats. The NMES group had more stable gait, neater footprints, higher muscle wet weight, more voluminous morphology and more regenerated muscle fibers. Additionally, ES treatment induced myogenic differentiation in rat MuSCs *in vitro*. Transcriptomic analysis also showed that "AMPK signaling pathway" was enriched and genes upregulated in ES-treated cells, revealing ES treatment could activate the autophagy in an AMPK-ULK1-dependent mechanism in MuSCs. Besides, it was also founded that infusion of AMPK or ULK1 inhibitor, knockdown of AMPK or ULK1 in MuSCs could block the effect of myotube formation of ES.

Conclusion: NMES not only restores muscle function but also enhances myogenic activity and muscle regeneration via AMPK-ULK1 autophagy in stroke-related sarcopenia rats. Our study provides a promising strategy for the treatment of stroke-related sarcopenia.

The translational potential of this article: This study first demonstrates that NMES alleviates stroke-related sarcopenia by promoting MuSCs differentiation through AMPK-ULK1-autophagy axis. The findings reveal a novel therapeutic mechanism, suggesting that NMES can restore muscle function and enhance regeneration in stroke patients. By combining NMES with MuSCs-based therapies, this approach offers a promising strategy for clinical rehabilitation, potentially improving muscle mass and function in stroke survivors. The translational potential

* Corresponding author. Department of Orthopedic Surgery, The First Affiliated Hospital of Soochow University, Suzhou, Jiangsu, 215006, China.
** Corresponding author. Department of Rehabilitation Medicine, Zhongshan Hospital Fudan University, Shanghai, 200032, China.
*** Corresponding author. Department of Rehabilitation Medicine, Zhongshan Hospital Fudan University, Shanghai, 200032, China.
E-mail addresses: lushunyi@suda.edu.cn (S. Lu), zhang.jian@zs-hospital.sh.cn (J. Zhang), lingtuisi@163.com (T. Fu).
[1] These authors contributed equally to this work.

https://doi.org/10.1016/j.jot.2025.03.021
Received 9 December 2024; Received in revised form 11 March 2025; Accepted 31 March 2025

lies in its applicability to non-invasive, cost-effective treatments for sarcopenia, enhancing patients' quality of life.

1. Introduction

Stroke, triggered by various factors such as hypertension, hypercholesterolemia, and carotid artery stenosis, has emerged as one of the most prevalent clinical conditions worldwide, affecting the quality of life and financial burden of patients [1,2]. Despite significant advancements in rehabilitation technology and medical equipment, many stroke patients experience stroke-related sarcopenia during recovery [3,4]. This condition is characterized by rapid structural muscle changes, differences in bilateral body performance caused by brain injury, and activation of catabolic signals as a result of neurotrophic imbalances [5]. Current clinical management strategies for stroke-related sarcopenia include rehabilitation, physical therapy, nutrition, medication, and hormone therapy [4]. However, further researches are required to determine the efficacy and safety of these approaches. Thus, the development of a reliable and feasible therapeutic strategy to enhance muscle function and increase muscle mass and fiber count in stroke-related sarcopenia is of great importance.

An increase in muscle mass and fiber count plays a key role in muscle regeneration [6]. Some studies have explored the use of costly growth factors in clinical and preclinical trials to promote muscle regeneration [7,8]. Skeletal muscle satellite cells, also known as muscle stem cells (MuSCs), are indispensable in the process of myogenic differentiation and skeletal muscle regeneration [9]. Notably, these cells exhibit significant myogenic potential, capable of differentiating into myoblast lineage cells to facilitate muscle regeneration. MuSCs has also been widely used in cell therapy because of its excellent differentiation capacity, including myoblasts, chondrocytes, cardiomyocytes, and hematopoietic lineages [10–15]. However, cell therapy using MuSCs still far been limited to open trauma related muscle diseases [16,17]. Interestingly, the myogenic potential of MuSCs can be regulated by various mechanical stimuli, such as extrinsic mechanical cues and suitable mechanical loads, particularly electrical stimulation (ES) [18–20]. ES has been utilized in cell culture systems and is known to affect various cell types. Moreover, ES has been found to accelerate neural stem cell differentiation into mature neurons [21,22]. Nonetheless, the underlying mechanisms behind the impact of ES on muscle regeneration remains largely unexplored.

Neuromuscular electrical stimulation (NMES) is a widely employed clinical rehabilitation technique that promotes recovery of muscle function through intermittent stimulation to induce muscle activity [23–26]. Notably, NMES treatment has been reported to promote muscle capacity during immobilization of human legs [27]. In addition, ES can promote increased MuSCs content and facilitate myogenic differentiation in rats, regardless of age, *in vitro* [28]. However, the underlying mechanisms behind NMES- and ES-induced myogenic differentiation remain unclear, and the concept of combining NMES with MuSCs has also yet to be proposed.

Autophagy, a type of regulated cell death, is a conserved biological process in eukaryotes that functions as a recycling mechanism, eliminating unwanted cytoplasmic components and organelles under specific physiological and pathological conditions [29–31]. Adenosine 5′-monophosphate-activated protein kinase (AMPK) plays a crucial role in many pathophysiological processes [32,33], such as regulation of cell proliferation, metabolic reprogramming, cell polarization, and participation in autophagy [34]. Unc-51-like kinase 1 (ULK1) has been reported as an essential downstream factor of the AMPK signaling pathway, promoting autophagy [35,36]. Previous studies have demonstrated that *in situ* ES of muscles can increase AMPK phosphorylation and activity in animals [37]. However, comprehensive mechanistic studies on the activation of the AMPK signaling pathway by NMES or ES have yet to be reported.

In the present study, we established rat stroke-related sarcopenia model and employed NMES as treatment. Notably, NMES treatment significantly improved muscle function, promoted myogenic activity and facilitated muscle regeneration in stroke-related sarcopenia rats. Additionally, we identified the AMPK-ULK1-autophagy axis as a crucial pathway in the promotion of myogenic differentiation in stroke-related sarcopenia rats after NMES treatment. Furthermore, we modeled this promotion of muscle regeneration by ES treatment via the AMPK-ULK1-autophagy axis *in vitro* using primary MuSCs. To the best of our knowledge, this is the first study to report the specific mechanism by which NMES and ES promote autophagy in MuSCs. Our study provides a novel approach for the future treatment of sarcopenia, utilizing NMES in conjunction with MuSCs.

2. Materials and methods

2.1. Rat model

In this study, permanent middle cerebral artery occlusion (pMCAO) was used to induce stroke-related sarcopenia in rats [38]. Briefly, rats were anesthetized with isoflurane gas (2–3 % inhaled). The rats were placed in a supine position, shaved, and disinfected; then, the left common carotid artery (CCA), internal carotid artery (ICA), and external carotid artery (ECA) were isolated. A suture (MSRC37B200PK50, RWD Life Science, China) was inserted into the ICA until it entered the head of the middle cerebral artery (MCA) (Figs. S1A and S1B). Cerebral blood flow (CBF) was monitored using laser Doppler flowmetry (PeriFlux6000, Perimed, Sweden). Rats with CBF values that decreased to <30 % were considered successful models. The neurological function of all rats was evaluated using the Zea-longa score 2 h after modeling [38]. Rats with Zea-longa scores of 1–3 were included in the study, while those with major bleeding, death, or subarachnoid hemorrhage were excluded. Confirmation of stroke-related sarcopenia was conducted using H&E staining and Catwalk gait analysis 48 h post-surgery (Fig. 1A to E; Movie S1 and S2). NMES treatment was initiated 48 h after surgery, targeting the muscles on the sarcopenic side, with daily 30-min sessions administered over seven consecutive days (Fig. S1C). Rats in the control group were connected to a machine without NMES treatment. At fourth and eighth weeks post-surgery, we employed the Catwalk Gait Analysis System to analyze the footprint mean intensity and footprint area of the hind limb on the sarcopenic side. All rats used in this study are Sprague–Dawley (SD) rats. The experiment involved two groups (n = 5 rats per group), with the entire protocol repeated three times independently to ensure reproducibility. All animal procedures were performed in accordance with the protocols approved by the Fudan University Institutional Animal Care and Use Committee (2023-044).

2.2. NMES treatment

NMES was administered to rats placed in a fixation device with both hind limbs exposed. Two somatic electrodes were positioned on the skin above the gastrocnemius muscle of the left leg and connected to a stimulator (XCH-B2, Shanghai NCC Electronics, China) for intermittent ES (pulse width: 200 μs, frequency: 20 Hz, on time: 5 s, off time: 10 s). The intensity of the current was adjusted to ensure visible movement of the toes, as a result of muscle contraction. Treated rats received NMES for 30 min/day for seven consecutive days. The rats showed no signs of NMES-induced pain or discomfort during muscle contractions.

2.3. The usage of CatWalk XT

An automated quantitative gait analysis system, CatWalk XT (CWT; Noldus, Wageningen, Netherlands), was used to assess the motor function and coordination of rats. Prior to the formal experiment, all rats underwent training to traverse the passage in the prescribed direction without hesitation. The CatWalk recordings were performed with exclusion of daylight, and each run consisted of at least two full-step cycles. The recorded runs were automatically classified with CatWalk XT Software 10.6.68 (Noldus, Wageningen, Netherlands) and manually processed as previously described [39–41]. Various gait parameters, including right and left print length, print width, print area, stride length, step cycle, stand, swing speed, and mean footprint intensity, were analyzed to assess coordination and identify differences between right and left paw prints.

2.4. Isolation of rat MuSCs and cell culture

Primary MuSCs were obtained from Sprague–Dawley rats (4–6 weeks old), as previously described [42]. Briefly, the EDL muscle was dissected from the hind limbs of these rats (Fig. S3A), and myofibers were isolated through collagenase II (2 mg/mL; Thermo Fisher Scientific, USA) digestion and trituration. Cells were then collected and cultured in DMEM medium (Thermo Fisher Scientific, USA) supplemented with 10 % (v/v) fetal bovine serum (OriCell, FBSSR-01021-500), and 1 % (v/v) penicillin-streptomycin (Thermo Fisher Scientific, USA) at 37 °C. Adherent cells were harvested at passage three for flow cytometry, where they were stained with fluorescence-labeled antibodies against Pax7 (NBP2-34706 PE, Novus, USA) and desmin (Y&M, BYK-1026R-FITC) (Fig. S3B). Rat MuSCs obtained from passages two and three were used for subsequent experiments (Fig. S3C).

After ES treatment, the culture medium was switched to DMEM supplemented with 2 % horse serum (S9050, Solarbio, China) to induce myogenic differentiation. Fresh medium was replaced two to three times per week, and myotube formation was observed after one week of differentiation.

2.5. ES treatment in vitro

For ES treatment, rat MuSCs were cultured in customized airtight chambers with air inlet and outlet channels in a CO2 cell incubator. Cells were seeded in dishes and plates at the following densities: 1.5 × 106 cells in a 10-cm dish, 2 × 105 cells/well in 6-well plates, and 4 × 104 cells/well in 24-well plates. Following one-day of growth, the MuSCs were stimulated using a DDS signal generator/counter (JDS6600, UMK, Guangdong, China) for 30 min with rectangular pulses. The voltage and duration of ES treatment varied according to the specific experiment, with these parameters being described in the corresponding figure legends.

2.6. H&E and Masson's trichrome staining

Following completion of the *in vivo* experiments, muscle tissues were fixed in 4 % paraformaldehyde (Servicebio, G1101) for 48 h at 4 °C (except for frozen sections). Then, fixed muscles were sectioned (4 μm thickness), and Masson's trichrome staining kit (Freethinking, FH115100) and H&E dye (Freethinking, FS141500) were used to visualize myofibers and collagen fibers in the muscle tissue.

2.7. Immunofluorescence

For tissue immunofluorescence analysis, paraffin sections were deparaffinized in xylene, hydrated in graded ethanol solutions, and subjected to heat-induced antigen retrieval. Endogenous peroxidases and antigens were then blocked with 3 % H2O2 and 3 % bovine serum albumin, respectively. The multiplex immunofluorescence protocol involved multiple rounds of staining, with each round involving incubation with the primary antibody followed by the secondary antibody. Finally, the nuclei were counterstained with DAPI. Antibodies against phospho-AMPK alpha (Thr172, #AF3423, CST, USA), phospho-ULK1 (Ser317, #AF2301, CST, USA), LC3B (14600-1-AP, Proteintech, China), PAX7 (20570-1-AP, Proteintech, China), and laminin (23498-1-AP, Proteintech, China) were used in this part of the study.

Control and ES-treated MuSCs and differentiated myotubes were visualized using primary and secondary antibodies. Antibodies against MyoD1 (#AF7733, CST, USA), PAX7 (20570-1-AP, Proteintech, China) and MYH6 (22281-1-AP, Proteintech, China) were used in this part of the study. Stained sections were observed under a fluorescence microscope (CKX53, Olympus, Japan).

2.8. Transcriptomic analysis

For transcriptomic analysis, primary MuSCs were cultured in complete growth medium until they reached confluence; subsequently, these cells were treated with ES stimulation or a control for 30 min. Total RNA was extracted using a TRIzol reagent kit (15596026, Thermo Fisher Scientific, USA) according to the manufacturer's instructions. The resulting cDNA library was sequenced by Gene Denovo Biotechnology, Guangzhou, China), using an Illumina Novaseq 6000 platform. Sequencing reads were mapped to the rat genome rn6 using HISAT2 [43], and tag counts were summarized at the gene level using SAMtools [44], thereby allowing only one read per position per length. DEGs were identified using DESeq2 [45]. These DEGs were then subjected to heatmap analysis using the R package pheatmap [46]. Finally, GO and KEGG gene set enrichment analysis of the DEGs was performed using clusterProfiler [47]. Additionally, GO analysis was performed using GOPlot [48].

2.9. Transmission electron microscopy

For transmission electron microscopy, control or ES-treated MuSCs were fixed with 2.5 % glutaraldehyde in 0.1 M sodium dihydrogen phosphatase (G1102, Servicebio, China) for 4 h at 4 °C before being fixed with 1 % osmium tetroxide for 1 h at room temperature. After dehydration using graded ethanol solutions and gradual infiltration with EMbed 812 epoxy resin (SPI, 90529-77-4), ultrathin sections (60–80 nm) were prepared using an ultramicrotome (Leica, EM UC7) and contrasted with 2 % uranium acetate and 2.6 % lead citrate. The sections were observed under a transmission electron microscope (Hitachi, HT7800) and autophagosomes were identified as previously described [49].

2.10. MuSCs transfection

Prepare lentivirus expressing shRNA targeting Prkaa1, Atg7 and Ulk1 (Hanbio, China). The lentiviruses were transduced into rat MuSCs using Polybrene (H8761, Solarbio, China). Subsequently, the transfected MuSCs were harvested or treated for 48 h after transfection. We chose the shRNA knock-out Prkaa1, Atg7 and Ulk1 mRNA for further animal experiments.

2.11. Autophagy flux detection

Prepare adenovirus expressing HBAD-mcherry-EGFP-LC3 (HB-AP2100001, Hanbio, China). After transduction, MuSCs were treated with ES or control conditions for 48 h. The cells were then fixed with 4 % paraformaldehyde (G1101, Servicebio, China) for 30 min at room temperature, and the nuclei were counterstained with DAPI (G1407-25 ML, Servicebio, China). Finally, immunofluorescence was observed and captured using a Leica SP8 Confocal microscope, as previously described [49].

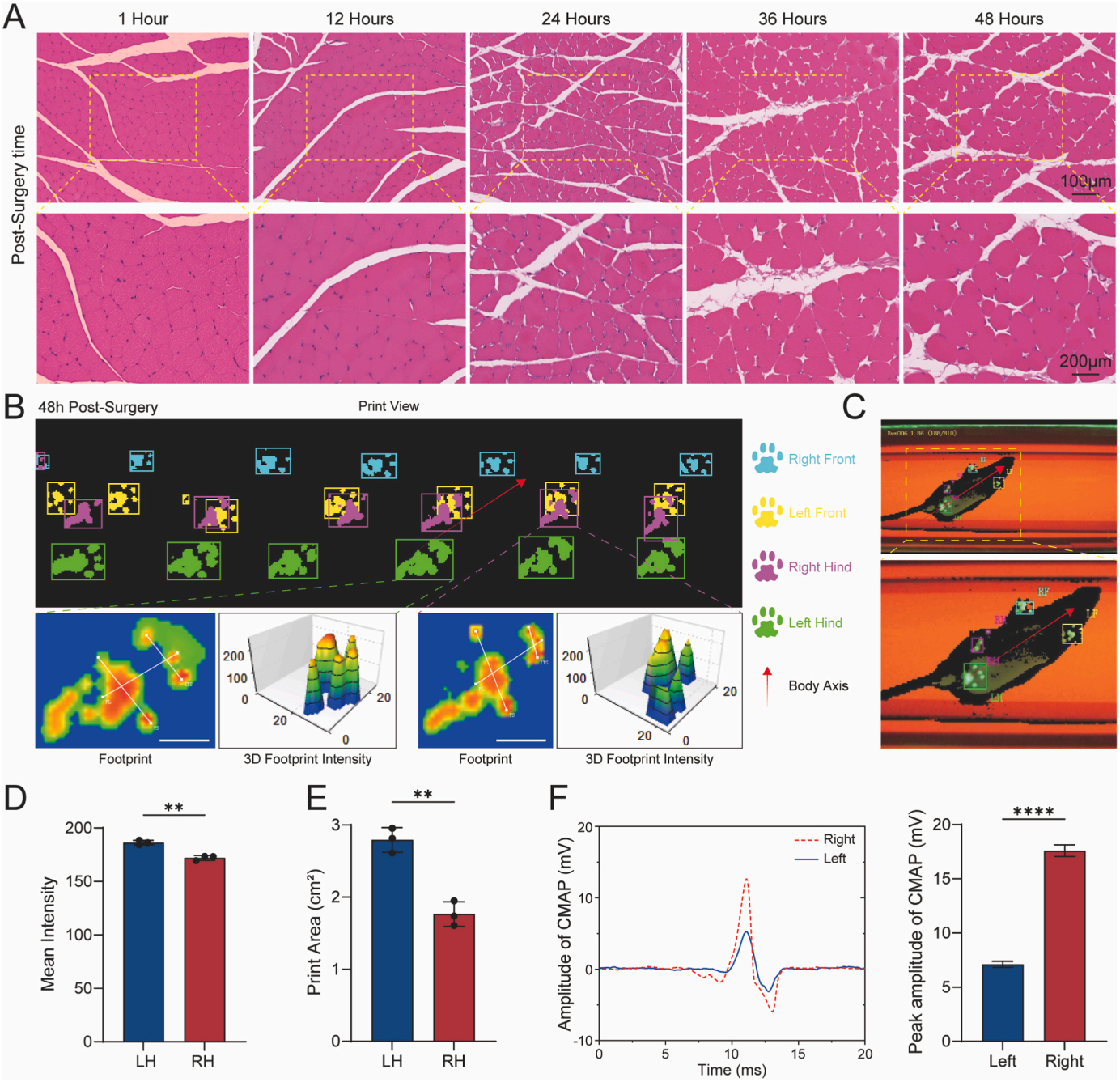

Fig. 1. Characterization of stroke-related sarcopenia. (A) Target muscle H&E staining at 1 h, 12 h, 24 h, 36 h and 48 h after surgery; scale bar: 100 μm. (magnification zones, scale bar: 200 μm). (B) Catwalk Footprint Gait Analysis of rat hind limbs in stroke-related sarcopenia rat. The dotted line magnified the footprint and displayed the peak footprint intensity; scale bar: 1 cm. (C) Image of stroke-related sarcopenia rat in the tunnel. (D) Quantitative analysis of the mean intensity of the left and right hind foot and (E) left hind foot print area (n = 3 in the control group and n = 3 in the NMES group; $^{**}P < 0.01$ by two-tailed unpaired Student's t test). (F) Amplitude of CMAP and quantitative peak amplitude of CMAP (n = 5 in each group; $^{****}P < 0.0001$ by two-tailed unpaired Student's t test).

2.12. Total RNA preparation and quantitative real-time PCR analysis

Total RNA was extracted from cultured MuSCs using TRIzol reagent (Thermo Fisher Scientific, 15596026, USA), according to the manufacturer's instructions. Then, 400 ng of total RNA was reverse transcribed into cDNA using a reverse transcriptase kit (4368814, Thermo Fisher Scientific, USA). qRT-PCR was performed using a SYBR green mixture (A25778, Thermo Fisher Scientific, USA) and a StepOnePlus Real-Time PCR instrument (4376600, Thermo Fisher Scientific, USA). Primers used for each transcript are listed in Table S1.

2.13. Co-immunoprecipitation and Western Blot

For Co-immunoprecipitation and Western Blot analysis, MuSCs (4 × 106 cells/sample) were collected and lysed in ice-cold RIPA lysis buffer (R0010, Solarbio, China) containing a protease inhibitor cocktail (04693124001, Merck, Germany) and a phosphatase inhibitor cocktail (04906845001, Merck, Germany). A few cell lysates were retained as inputs. Next, AMPKα antibody (#5831, CST, USA) and protein A-G magnetic beads (HY-K0202, MedChemExpress, USA) were then used to perform immunoprecipitation. Cell lysates were then centrifuged at 12000×*g* for 15 min at 4 °C, and the protein sample was diluted for

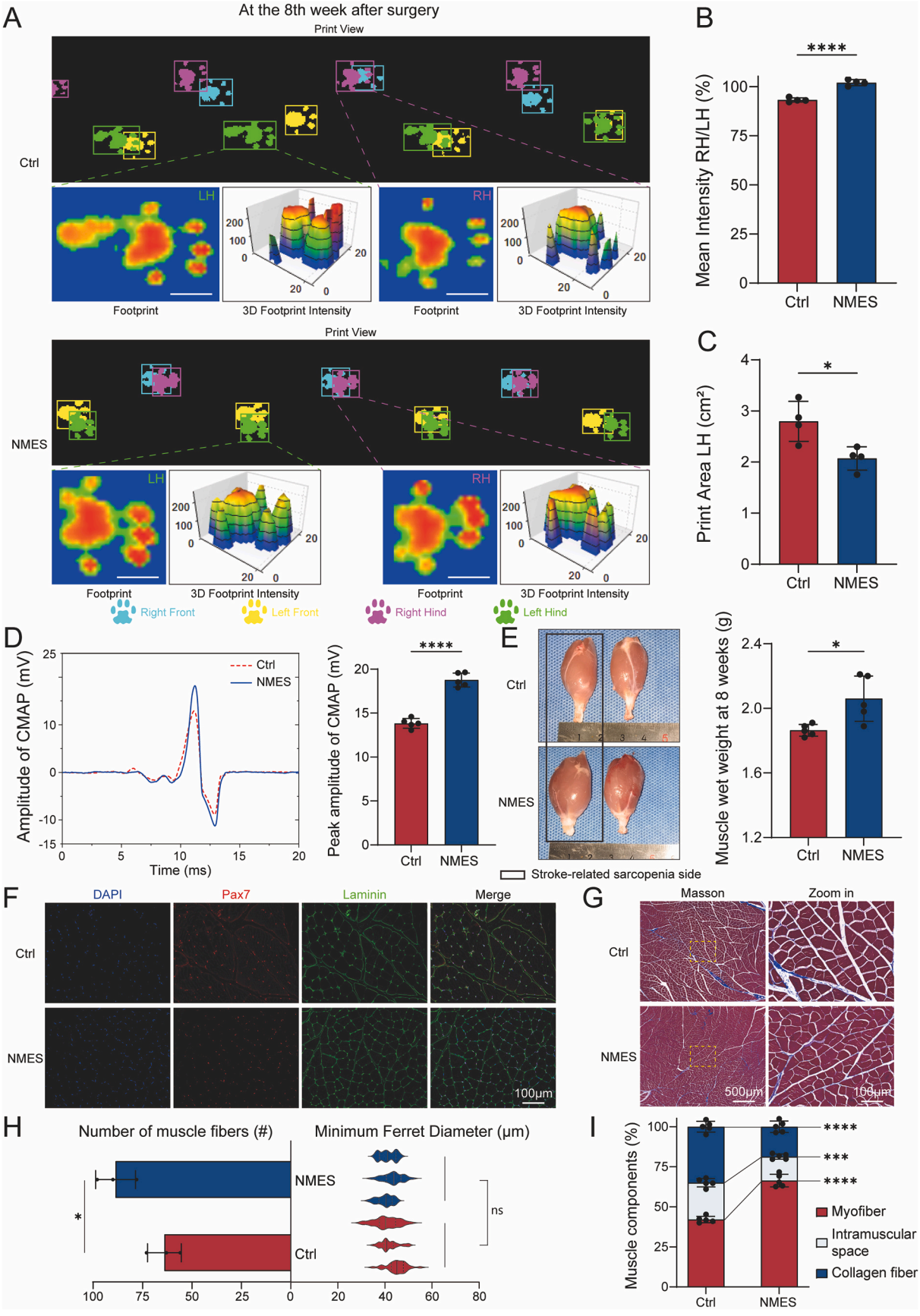

(caption on next page)

Fig. 2. NMES accelerated muscle regeneration and functional recovery in rats with stroke-related sarcopenia. (A) Catwalk Footprint Gait Analysis of rat hind limbs in the control and NMES groups eight weeks after surgery. The dotted line magnified the footprint and displayed the peak footprint intensity; scale bar: 1 cm. (B) Quantitative analysis of the mean intensity of the right/left hind foot and (C) left hind foot print area (n = 4 in the control group and n = 4 in the NMES group; *P < 0.05, ****P < 0.0001 by two-tailed unpaired Student's t test). (D) Amplitude of CMAP and quantitative peak amplitude of CMAP (n = 5 in each group; ****P < 0.0001 by two-tailed unpaired Student's t test). (E) Target muscle general images and quantitative analysis showing muscle wet weight (n = 5 in each group; *P < 0.05 by two-tailed unpaired Student's t test). (F) Immunofluorescence of Pax7 and Laminin in muscle with stroke-related sarcopenia from the control and NMES groups; scale bar: 100 μm. (G) Masson's trichrome staining of muscle eight weeks after surgery. Dotted squares indicated magnification zones; scale bar: 500 μm (for magnification, scale bar: 100 μm). (H) ImageJ software evaluated the number and average diameter (Ferret diameter) of muscle fibers in a random field of view from F-panel (n = 3 in each group; *P < 0.05 and ns by two-tailed unpaired Student's t test). (I) Quantitative analysis of the myofiber, intramuscular space and collagen fiber in the Masson's trichrome staining from G-panel (n = 5 in each group; ***P < 0.001, ****P < 0.0001 by two-tailed unpaired Student's t test).

denaturation. Subsequently, 50 μg of total sample protein was separated using 10 % SDS-PAGE and electrotransferred onto polyvinylidene fluoride membranes using a Bio-Rad power supply (CA, USA). The membranes were then incubated with primary antibodies and horseradish peroxidase-conjugated secondary antibodies (A0208, Beyotime, China). Protein bands were visualized using an ECL kit (34580, Thermo Fisher Scientific, USA). Images were captured using an enhanced chemiluminescence imaging system (ChemiDoc XRS+, Bio-Rad, USA) with default parameters and without gamma adjustment. Subsequently, images were analyzed using the Image Lab analysis software (#1709690, Bio-Rad, USA). GAPDH was used as the loading control. Uncropped Western Blots used in this study are summarized in Data S1. Antibodies against AMPKα (#5831, CST, USA), ULK1 (#8054, CST, USA), mTOR (#2972, CST, USA), phospho-mTOR (Ser2448) (#2971, CST, USA), AMPK alpha (#AF6423, CST, USA), phospho-AMPK alpha (Thr172) (#AF3423, CST, USA), ULK1 (#DF7588, CST, USA), p-Ser317-ULK1 (#AF2301, CST, USA), and p-Ser757-ULK1 (#AF4387, CST, USA), P62 (18420-1-AP, Proteintech, China), ATG7 (10088-2-AP, Proteintech, China), light chain-specific (SA00001-7L, Proteintech, China), and GAPDH (60004-1-Ig, Proteintech, China) were used in this part of the study.

2.14. Statistical analysis

Quantitative data are presented as the mean ± SD. Individual data points are displayed, and all experiments were performed with at least three replicates. Statistical analysis was performed using the unpaired Student's t-test for comparisons between two groups. For comparisons of more than two groups, one-way analysis of variance (ANOVA) was used, followed by Bonferroni multiple comparisons post-hoc test. For experiments that considered two factors, we employed a two-way ANOVA followed by Tukey's multiple comparison test. The areas of fluorescent staining for muscle fibers and nuclei were quantified using ImageJ software. Data were analyzed using GraphPad Prism software (version 9.0, USA). A P value < 0.05 was considered statistically significant.

3. Results

3.1. Characterization of stroke-related sarcopenia

To determine whether NMES can promote muscle regeneration and functional recovery, we employed a rat model of permanent middle cerebral artery occlusion (pMCAO)-induced stroke-related sarcopenia (Figs. S1A and S1B). The rats developed a right-sided stroke with left-sided hemiparesis and stroke-related sarcopenia. Confirmation of stroke-related sarcopenia was established through hematoxylin and eosin (H&E) staining and CatWalk gait analysis conducted 36–48 h post-surgery, and this was accompanied by diminished compound muscle action potentials (CMAP) on the stroke-related sarcopenia side. H&E staining showing distinct stroke-related sarcopenia in the ipsilateral hindlimb at 36–48 h post-surgery (Fig. 1A). CatWalk gait analysis revealed significant interlimb asymmetry, with the affected left hindlimb exhibiting higher paw mean intensity (14.31 ± 1.769 units) and larger paw print area (1.028 ± 0.1404 cm^2; Fig. 1B to E) compared to the contralateral limb. Electrophysiological measurements further showed a reduction in CMAP amplitude in the ipsilateral gastrocnemius (10.48 ± 0.2705 mV; Fig. 1F). Additionally, the rats exhibited a characteristic hemiplegic gait (lateral rotation) (Movie S1 and S2). These results demonstrated that the stroke-related sarcopenia rat model was successfully established.

Supplementary data related to this article can be found online at https://doi.org/10.1016/j.jot.2025.03.021

Video 1.

Video 2. 3

3.2. NMES accelerated muscle regeneration and functional recovery in stroke-related sarcopenia rats

Visual examination revealed that rats in the NMES group exhibited a more stable gait with neater footprints. Notably, the footprint intensities and areas of the NMES group were considerably lower than those of the control group at eight weeks post-surgery (Fig. 2A). Quantitative analysis further demonstrated that the NMES group exhibited a significantly higher mean intensity ratio of the healthy side (right) to the sarcopenic side (left), and a smaller print area compare to the control group (Fig. 2B and C). Overall, rats with poorer muscle recovery showed significantly higher print intensity, smaller RH/LH ratios (8.805 ± 0.9192 %; Fig. 2B), and larger footprint areas (0.7259 ± 0.2265 cm^2; Fig. 2C). Moreover, compared to the control group, the NMES group displayed higher CMAP peaks (4.938 ± 0.4343 mV; Fig. 2D). Notably, the CMAP of the NMES-treated side exhibited no significant difference from that of the healthy side within the same rat eight weeks post-surgery (Fig. S2F). Examination of muscles *in vitro* revealed that the NMES group exhibited approximately 10 % higher wet muscle weight and a more robust morphology than that observed in the control group (0.1960 ± 0.06493 g; Fig. 2E). Moreover, immunofluorescence analysis demonstrated that the NMES group displayed a greater abundance of regenerated muscle fibers (Fig. 2F). Utilizing ImageJ software, we calculated the number and average diameter (Feret diameter) of muscle fibers in random fields of view. Quantitative analysis revealed no significant difference in the minimum Feret diameter of muscle fibers between the two groups; however, the NMES group exhibited a higher number of muscle fibers (24.67 ± 7.623 count per field; Fig. 2H). Furthermore, Masson's trichrome staining indicated a significant increase in muscle myofibers and a significant decrease in interstitial space and collagen in the NMES group (Fig. 2G and I). Similar trends were also observed in rats at four weeks post-surgery (Figs. S2A–S2E). Overall, these results suggested that NMES significantly improved muscle mass and promoted muscle regeneration *in vivo*.

3.3. ES promoted myogenic differentiation of rat MuSCs

To further confirm the impact of NMES on muscle regeneration, we utilized custom-designed cell culture well plates equipped with a signal generator (ES apparatus) to simulate NMES *in vitro* (Fig. 3A). We isolated primary rat MuSCs from extensor digitorum longus (EDL) muscle tissue (Fig. S3A) and confirmed their identity through flow cytometry, with these cells exhibiting positive staining for MuSCs markers, paired box 7 (Pax7), and desmin (Fig. S3B) [50]. To determine the optimal ES

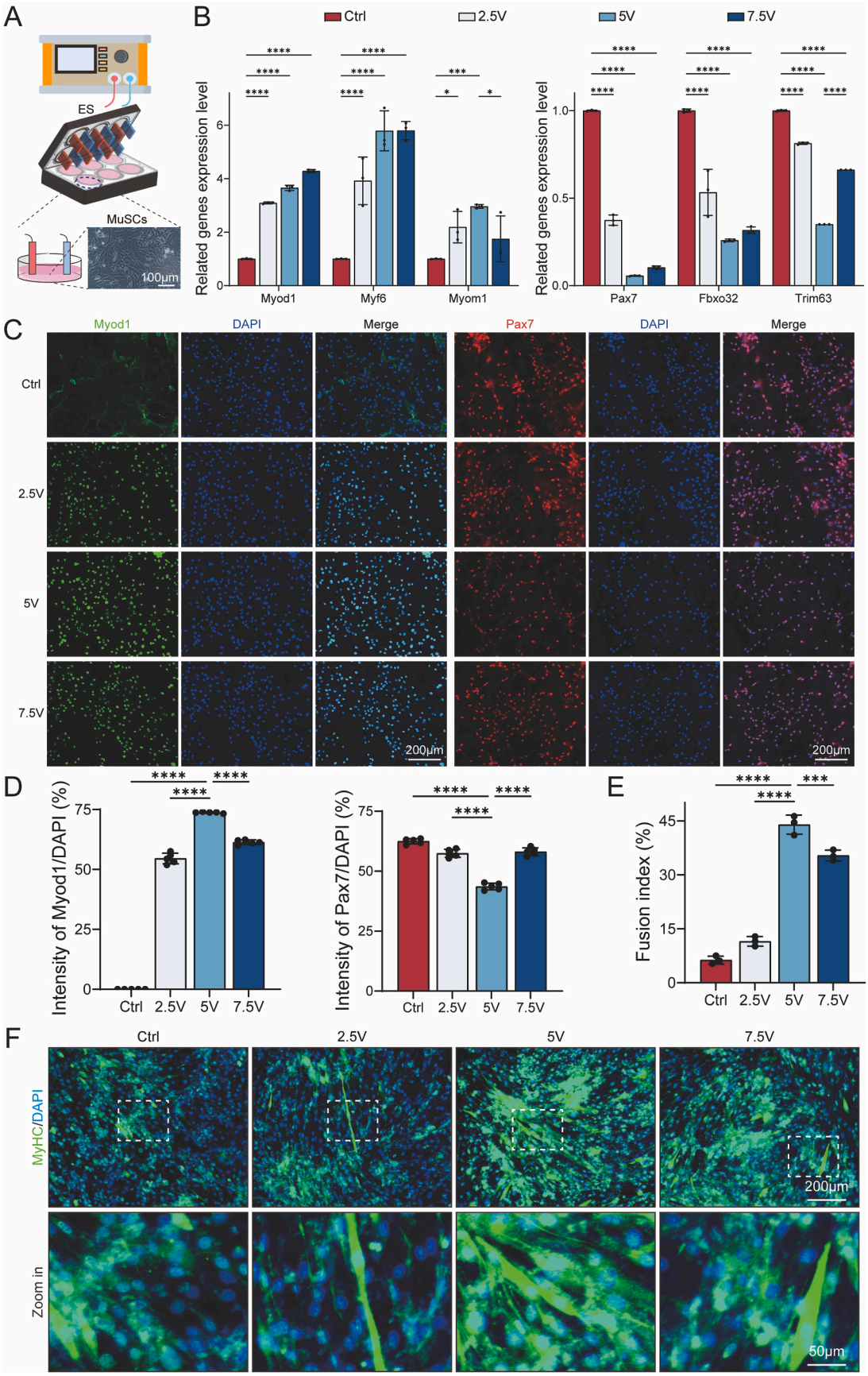

(caption on next page)

Fig. 3. ES promoted myogenic differentiation of rat MuSCs. (A) Illustration of ES treatment *in vitro*. (B) Relative expression levels of muscle differentiation-related genes (Myf6, Myod1, Myom, Pax7, Fbxo32, Trim63) in MuSCs under different voltages for 30min measured by qRT-PCR (n = 3 in each group; relative to Gapdh; $^{*}P < 0.05$, $^{***}P < 0.001$ $^{****}P < 0.0001$ by one-way ANOVA, followed Bonferroni multiple comparisons post-hoc test). (C) Immunofluorescence staining for Myod1 (green), Pax7 (red) and DAPI (blue) in MuSCs under control and different voltages for 30min; scale bar: 200 μm. (magnification zones, scale bar: 50 μm) (D) Quantitative analysis of immunofluorescence intensity for Myod1 and Pax7 at various voltages (three random filed in each group; $^{****}P < 0.0001$ by one-way ANOVA and Bonferroni multiple comparisons post-hoc test). (E) MuSCs after ES treatment incubated in differentiation medium for three days, before immunostaining for myosin heavy chain (MyHC, MYH6) (green) and counterstained with DAPI (blue); scale bar: 200 μm. (F) Quantitative analysis of immunofluorescence intensity for MyHC of the E-panel (three random filed in each group; $^{***}P < 0.001$, $^{****}P < 0.0001$ by two-way ANOVA, followed by Tukey's multiple comparisons test)

parameters for MuSCs differentiation, we employed voltage-controlled square unipolar pulses (pulse width: 200 μs, frequency: 20 Hz) with varying voltages to stimulate the MuSCs. Under the different ES conditions, rat MuSCs were induced to initiate differentiation, and eventually differentiated into myotubes. During ES treatment, the expression levels of proteins and genes associated with myogenic differentiation could be modulated by adjusting the voltage.

Quantitative real-time PCR (qRT-PCR) results also confirmed the expression of multiple muscle differentiation–related genes, ultimately demonstrating the upregulation of myoblast differentiation genes Myod1, Myf6, and Myom1, alongside the downregulation of myoblast differentiation inhibition–related genes Pax7, Fbxo32, and Trim63 (Fig. 3B). Immunofluorescence analysis further confirmed the upregulation of Myod1 expression and downregulation of Pax7 expression (Fig. 3C and D). Notably, cells treated with 5 V of ES displayed the highest level of Myod1 expression, the lowest level of Pax7 expression, and superior myotube formation (Fig. 3E and F). Ultimately, these findings confirmed the efficacy of ES in promoting the myogenic differentiation of rat MuSCs *in vitro*.

3.4. Transcriptomic analysis of rat MuSCs undergoing ES-induced myogenic differentiation

To elucidate the underlying mechanism by which ES promotes myogenic differentiation of rat MuSCs, we performed RNA sequencing (RNA-seq). Volcano plot analysis identified 1359 differentially expressed genes (DEGs) post-ES treatment, comprising 852 upregulated and 507 downregulated genes (Fig. 4A and B). Gene Ontology (GO) analysis further highlighted a significant enrichment of genes associated with muscle regeneration (Fig. 4C). Subsequently, the enriched terms related to the myogenic effects of ES were subjected to GO Chord analysis, categorizing genes into the following groups: "muscle cell differentiation," "regulation of actin cytoskeleton organization," "striated muscle cell differentiation," "muscle cell migration," "actin polymerization or depolymerization," and "muscle cell proliferation" (Fig. 4D). Consistently, the upregulated expression of myogenesis-promoting genes, such as Myf6, Myod1, Myom1, and Des, alongside the downregulated expression of Trim63 and Fbxo32 were verified by qRT-PCR (Fig. 4E). These results collectively suggested that systemic ES treatment induces myogenic differentiation of rat MuSCs.

3.5. AMPK mediated the myogenic role of ES

To explore the initial driver of the myogenic effects induced by ES treatment, we conducted Kyoto Encyclopedia of Genes and Genomes (KEGG) enrichment analysis. Enrichment in the AMPK signaling pathway was of particular note since AMPK is a key sensor of oxidation–reduction and energy metabolism (Fig. 5A) [32,33]. Immunofluorescence analysis revealed heightened phosphorylation of 5′-AMP-activated catalytic subunit alpha (PRKAA/AMPKα) at Thr172 in MuSCs derived from stroke-related sarcopenia muscles in the NMES group compared with those from the control group (Fig. 5B). This observation was further validated by Western Blotting, with ES-treated cells displaying increased PRKAA phosphorylation compared to that observed in control cells (Fig. 5C).

To determine whether PRKAA activation is sufficient to elicit the effects on myogenic differentiation associated with ES, we treated rat MuSCs with the PRKAA inhibitor compound C (BML-275) and the agonist acadesine (AICAR). While ES effectively promoted PRKAA phosphorylation, addition of BML-275 reversed the effect of ES on PRKAA phosphorylation (Fig. 5D). Conversely, AICAR effectively stimulated PRKAA phosphorylation and normalized the difference between the two groups (Fig. 5D). Importantly, BML-275 effectively eliminated the effects of ES on myogenesis. In contrast, AICAR markedly enhanced ES-induced myotube formation (Fig. 5E and F). To validate the specific requirement of PRKAA for ES-induced myogenic differentiation, we employed a knockdown of 5′-AMP-activated catalytic subunit alpha 1 (Prkaa1) using shRNA, as Prkaa1 expression was determined to be much higher than 5′-AMP-activated catalytic subunit alpha 2 (Prkaa2) in our MuSCs transcriptome dataset (Figs. S4A and S4B). This Prkaa1 knockdown (Fig. S4C) was found to abrogate the enhanced myoblast differentiation induced by ES treatment, as evidenced by diminished myotube formation (Fig. 5G and H) and reduced expression of myogenesis-related genes (Fig. S4D). In summary, these findings suggested that ES treatment promotes myogenic differentiation by activating AMPK signaling.

3.6. AMPK activation induced autophagy during ES-induced myogenic differentiation

AMPK activation affects various biological processes, including autophagy [35,36,51]. Interestingly, GO analysis demonstrated that the genes upregulated in ES-treated cells were significantly enriched in the biological and cellular processes of autophagy (Fig. S5A). Furthermore, as detected by transmission electron microscopy, ES-treated cells exhibited a higher abundance of autophagosomes compared to the control group (Fig. 6A). Activation of autophagic flux in ES-treated cells was further confirmed by a decreased ratio of microtubule-associated protein 1 light chain 3 beta (LC3B/MAP1BLC3B) yellow puncta to total LC3B red puncta in comparison to that of the control cells (Fig. 6C and D). LC3B is involved in phagophore expansion, and its acidic- and/or proteolytic-sensitive GFP-tagged signal was decrased during autolysosome formation [49]. Increased autophagy was also observed in MuSCs from stroke-related sarcopenic muscles of the NMES group by immunofluorescence staining for LC3B and Pax7 (Fig. 6E). Correspondingly, Western Blot analysis revealed elevated levels of ubiquitin-like modifier-activating enzyme (ATG7), LC3B-I, and LC3B-II, alongside reduced levels of ubiquitin-binding protein p62 (P62) in ES-treated rat MuSCs (Fig. 6B), indicating autophagosome formation and degradation [49].

To explore whether AMPK activation drives autophagy, we administered the AMPK inhibitor BML-275 to ES-treated cells. BML-275 effectively reduced ATG7, LC3B-I, and LC3B-II levels while increasing P62 levels in both ES-treated and control groups to comparable levels (Fig. S5B). These findings highlight the involvement of PRKAA activation–mediated autophagy in ES-induced myogenic differentiation. To further determine whether autophagy is required for ES-induced myogenic differentiation, we treated rat MuSCs with two autophagic inhibitors, chloroquine and bafilomycin A1. These inhibitors impeded autophagic flux by inducing the accumulation of P62 and LC3B-II (Fig. 6F), thereby eliminating the stimulatory effect of ES on myogenic differentiation (Fig. 6G and H). To establish the specific requirement for autophagy in ES-induced myogenic differentiation, we conducted

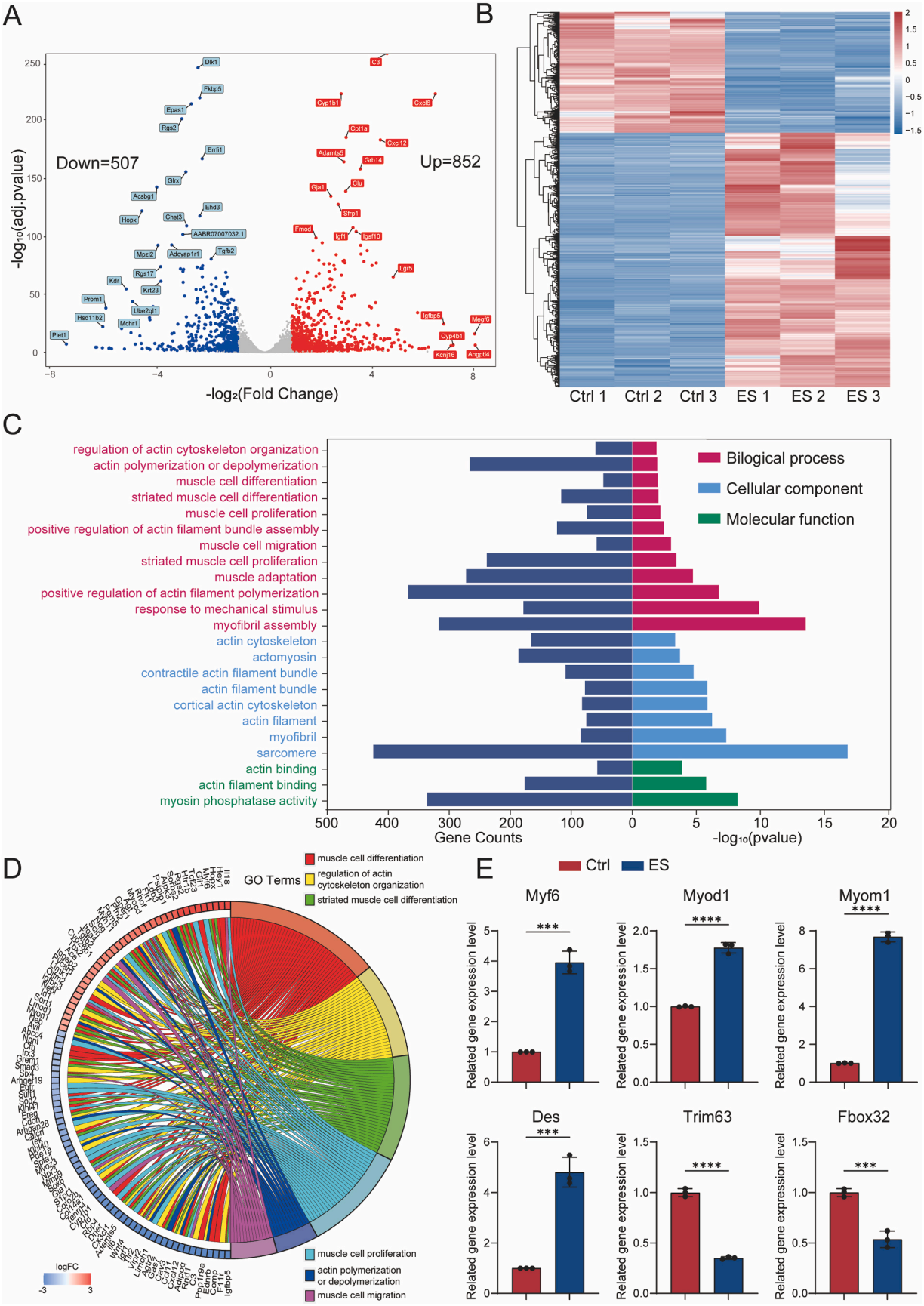

(caption on next page)

Fig. 4. Transcriptomic analysis of rat MuSCs undergoing ES-induced myogenic differentiation. (A) Volcano map of the RNA-seq data of MuSCs in the control versus ES (5V treatment for 30min) groups calculated by DESeq2 (n = 3 in each group). (B) Heatmap of DEGs for MuSCs in the Control versus ES groups (n = 3 in each group). (C) Biological process, Cell component and Molecular function three in one double-sided bar chart of Gene Ontology (GO) enrichment analysis of the DEGs. (D) GOChord plot of GO enrichment analysis, displaying of the relationship between genes and the following terms: "muscle cell differentiation", "regulation of actin cytoskeleton organization", "striated muscle cell differentiation", "muscle cell migration", "actin polymerization or depolymerization", and "muscle cell proliferation". (E) Verification of DEGs (Myf6, Myod1, Myom1, Des, Trim63 and Fbox32) in MuSCs from the control and ES groups measured by qRT-PCR (n = 3 in each group; relative to Gapdh; $^{***}P < 0.001$, $^{****}P < 0.0001$ by two-tailed unpaired Student's t test).

knockdown experiments in MuSCs, targeting Atg7, a critical factor in autophagy (Fig. S5C) [52]. Consistently, downregulation reversed the effects of ES on myogenesis, resulting in reduced myotube formation (Fig. 6I and J) and decreased expression of myogenesis-related genes (Fig. S5D). Overall, these findings suggest that PRKAA activation–mediated autophagy is required for ES to promote myogenic differentiation.

3.7. AMPK phosphorylation of ULK1 was required for ES-induced autophagy and myogenic differentiation

To further explore the effect of AMPK activation on autophagy, we examined the phosphorylation status of ULK1 and mammalian target of rapamycin (mTOR), two essential downstream factors of AMPK signaling involve in autophagy regulation [35,36]. It was founded that elevated levels of p-Ser317-ULK1 were founded in ES-treated MuSCs (Fig. 7A). Similarly, phosphorylation of ULK1 at Ser317 was significantly increased in stroke-related sarcopenic MuSCs in NMES-treated rats (Fig. 7B). However, mTOR phosphorylation did not change apparently (Fig. S6A). Moreover, no significant changes in p-Ser757-ULK1 expression were detected (Fig. S6B). Nonetheless, co-immunoprecipitation experiments revealed the interaction between PRKAA and ULK1 (Fig. 7C).

To determine whether ULK1 mediates the effects associated with ES treatment, we employed the ULK1 inhibitor SBI-0206965 (SBI) or the agonist BL-918 in conjunction with ES treatment. The results showed that ES-induced activation of PRKAA was not associated with SBI or BL-918. Nonetheless, SBI strongly suppressed ES-induced phosphorylation of ULK1 and formation of LC3B-II (Fig. 7D). In contrast, when treated with BL-918 alone, MuSCs maintained high levels of ULK1 phosphorylation and LC3B-II production, which enhanced the autophagy-promoting effect of ES treatment (Fig. 7D). Consistently, SBI inhibited the effects of ES on myotube formation, whereas BL-918 enhanced myogenic differentiation following ES treatment (Fig. 7E). Moreover, shRNA knockdown of Ulk1 (Fig. S6C) reversed the enhanced myogenesis induced by ES treatment, as evidenced by reduced myotube formation compared with control cells (Fig. 7G), alongside decreased expression of myogenesis-related genes (Fig. S6D). Notably, SBI effectively antagonized ULK1 activation and LC3B-II formation induced by the PRKAA agonist AICAR (Fig. 7H). Moreover, SBI effectively abrogated the effects of ES and AICAR on myotube formation (Fig. 7I).

Finally, to verify the activation of the corresponding signaling pathway *in vivo* by NMES treatment, protein expression *in vivo* was also validated by applying lentiviral shRNA knockdown of the corresponding gene to rats (Fig. 7 F). These findings suggest that ULK1 mediates the effects of ES on myogenic differentiation by acting downstream of PRKAA.

4. Discussion

Stroke-related sarcopenia is a newly recognized disease that has been rarely studied to date. Compared to photochemical methods, the thread ligation method (MCAO) produces animal models that closely mimic the characteristics of human ischemic stroke, particularly with regard to the absence of early vascular source edema in rat smoke models. Moreover, it allows the simulation of reperfusion injuries [38,53]. Notably, our research represents a pioneering effort to establish a rodent model of stroke-related sarcopenia, distinct from prior stroke models that focused solely on neurological deficits. While gait speed is a widely accepted diagnostic criterion for human sarcopenia [54], we evaluated sarcopenia in rats using gait analysis parameters (print area, mean intensity) combined with histopathological evidence from hematoxylin-eosin (H&E) staining (Fig. 1A to E), which revealed characteristic muscle atrophy and fiber disorganization. These criteria align with the European Working Group on Sarcopenia in Older People (EWGSOP) guidelines [54], adapted for rodents by emphasizing functional mobility and structural degeneration. Nevertheless, we recognize the limitations of relying solely on these metrics. Future studies would benefit from incorporating advanced techniques such as muscle ultrasound to quantify echogenicity or electromyography to assess neuromuscular function, which could refine diagnostic thresholds and enhance translational validity. Understanding rodent sarcopenia behavior is critical for elucidating human pathogenesis due to conserved physiological mechanisms. Rodents share key molecular pathways governing muscle protein synthesis, mitochondrial dysfunction, and neurovascular regulation with humans [55,56]. For instance, post-stroke inflammation and disuse atrophy in our model mirror the multifactorial etiology of human stroke-related sarcopenia. Rodent models allow controlled exploration of temporal disease progression and therapeutic interventions, which is ethically or practically challenging in clinical studies. Moreover, gait abnormalities in rats, analogous to slowed walking speed in humans, serve as functional biomarkers linking species-specific sarcopenic phenotypes [57].

NMES treatment, which involves intermittent ES to activate muscle activity, has emerged as a widely employed rehabilitation technique in clinical practice for promoting muscle function recovery [23–26]. However, existing studies have primarily focused on identifying the optimal parameters for NMES treatment across various diseases, with limited attention given to elucidating its underlying mechanisms.

MuSCs play a key role in myogenic differentiation and skeletal muscle regeneration [9], owing to their extensive myogenic potential and capacity to differentiate into myoblast lineage cells [13–15]. Under normal resting conditions, MuSCs express Pax7, but not MyoD1 [58,59], with Pax7 inducing proliferation and repressing differentiation [60–62]. Conversely, quiescent satellite cells enter the cell cycle and begin to express MyoD1, accompanied by a decline in Pax7 expression [50,63,64]. Therefore, we employed Pax7 as a marker for primary MuSCs. Given the crucial role of promoting myogenic differentiation in increasing muscle mass and fiber count [6,9], there is an urgent need for treatments that target this process to replace the expensive growth factors currently used in therapeutic techniques [7,8]. Previous research has proposed the use of MuSCs for cell therapy due to their multi-lineage differentiation potential [10–14]. Additionally, it has been demonstrated that the myogenic potential of MuSCs can be modulated by ES [20]. However, the potential application of NMES or ES treatment to activate myogenic differentiation in MuSCs to promote muscle regeneration has not been previously explored. ES treatment has been reported to promote muscle capacity [27], increases MuSCs content, and promotes myogenic differentiation *in vitro* [28]. In the present work, our study provides insights into a promising therapeutic approach involving combination therapy using NMES and MuSCs, with the aim of enhancing myogenic activity, promoting muscle regeneration, and restoring muscle function *in vivo*. In particular, this therapeutic approach primarily focuses on addressing muscle mass loss in stroke-related sarcopenia. We determined the optimal parameters (pulse width: 200 μs, frequency: 20 Hz, input: 5 voltage) of ES treatment for inducing myogenic

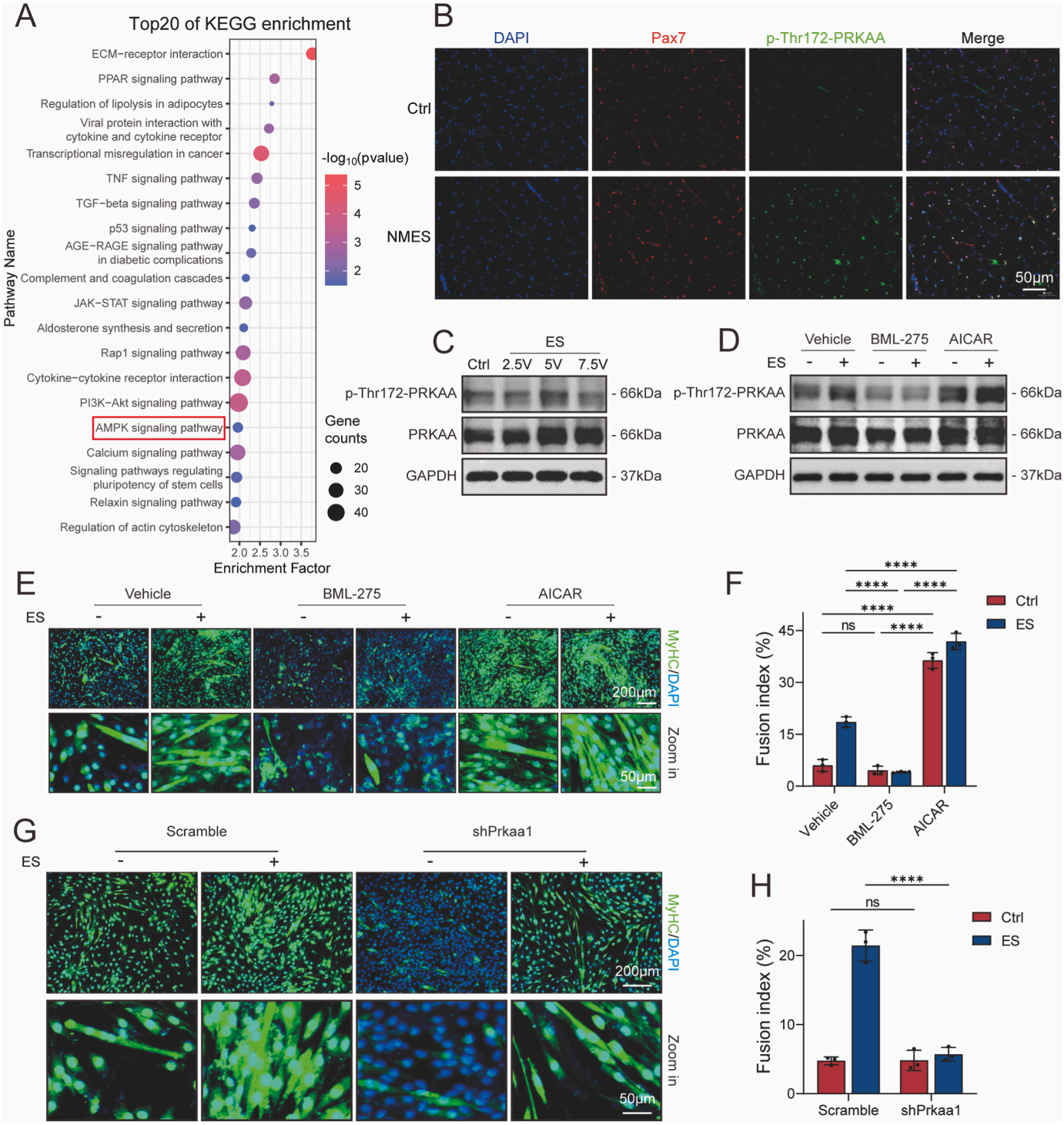

Fig. 5. AMPK mediated the myogenic role of ES. (A) KEGG enrichment analysis of DEGs (KEGG disease pathway filtered). (B) Immunofluorescence staining for p-Thr172-PRKAA, Pax7 and DAPI in muscle with stroke-related sarcopenia from control group and NMES-treated group; scale bar: 50 μm. (C) Western Blot analysis of PRKAA activation in MuSCs under control and different voltages for 30min. (D) Western Blot analysis of PRKAA activation in MuSCs pretreated with PRKAA inhibitor BML-275 (0.2 μM) or agonist AICAR (15 μM) for 24h in control group and ES treatment (5V treated for 30min) group. (E) Immunofluorescence staining of MuSCs after myotube differentiation for three days with BML-275 or AICAR in control group and ES treatment group. MyHC (green) and DAPI (blue) for myotube; scale bar: 200 μm (magnification zones, scale bar: 50 μm). (F) Quantitative analysis of immunofluorescence intensity for MyHC of the E-panel (three random filed in each group; $^{****}P < 0.0001$ by two-way ANOVA, followed by Tukey's multiple comparisons test). (G) Immunofluorescence staining of MuSCs after myotube differentiation for three days infected with scramble or shPrkaa1 lentivirus in control group and ES treatment group; scale bar: 200 μm (magnification zones, scale bar: 50 μm). (H) Quantitative analysis of immunofluorescence intensity for MyHC of the G-panel (three random filed in each group; $^{****}P < 0.0001$ by two-way ANOVA, followed by Tukey's multiple comparisons test).

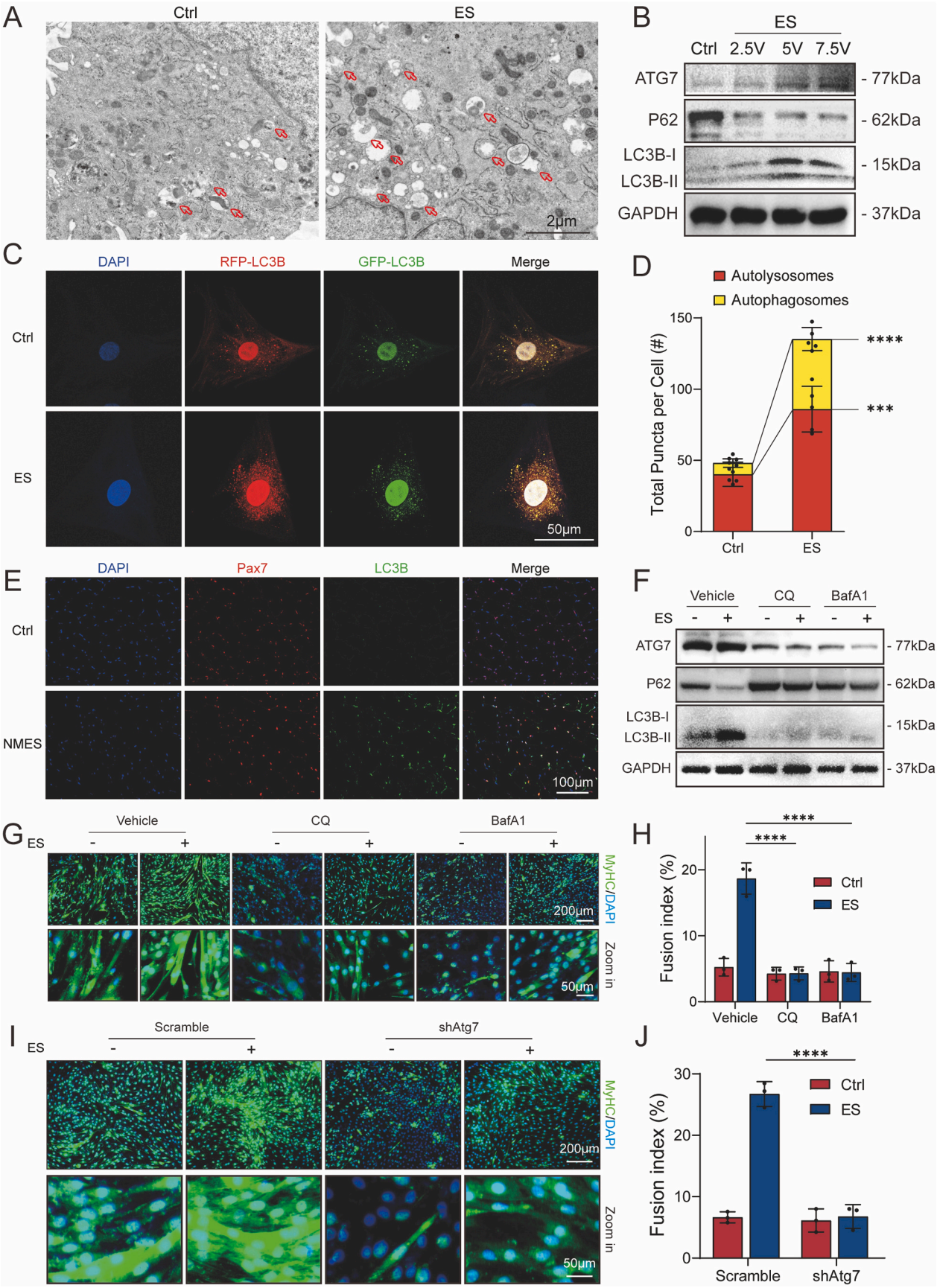

(caption on next page)

Fig. 6. AMPK activation caused autophagy during ES-induced myogenic differentiation. (A) Transmission electron microscopy of MuSCs in control group and ES treatment group. Arrows indicated autophagosomes; scale bar: 2 μm. (B) Western Blot analysis of autophagic activation in MuSCs under control and different voltages for 30min. (C) Autophagic flux detection for MuSCs transfected with HBAD-mcherry-EGFP-LC3 in control group and ES treatment group; scale bar: 50 μm. (D) Quantitative analysis of the autophagic flux in B-panel (n = 5 in each group; ***$P < 0.001$, ****$P < 0.0001$ by two-tailed unpaired Student's t test). (E) Immunofluorescence staining for LC3B, Pax7 and DAPI in muscle with stroke-related sarcopenia from control and NMES-treated rats; scale bar: 100 μm. (F) Western Blot analysis of autophagic activation in the MuSCs treated with autophagy inhibitors chloroquine (CQ, 40 μM) or bafilomycin A1 (BafA1, 1.5 μM) under control and ES conditions. (G) Immunofluorescence staining of MuSCs after myotube differentiation for three days with CQ or BafA1 under control and ES conditions; MyHC (green) and DAPI (blue) for myotube; scale bar: 200 μm (magnification zones, scale bar: 50 μm). (H) Quantitative analysis of immunofluorescence intensity for MyHC of the G-panel (three random filed in each group; ****$P < 0.0001$ by two-way ANOVA, followed by Tukey's multiple comparisons test). (I) Immunofluorescence staining of MuSCs after myotube differentiation for three days infected with scramble or shAtg7 lentivirus in control group and ES treatment group; MyHC (green) and DAPI (blue) for myotube; scale bar: 200 μm (magnification zones, scale bar: 50 μm). (J) Quantitative analysis of immunofluorescence intensity for MyHC of the E-panel (three random filed in each group; ****$P < 0.0001$ by two-way ANOVA, followed by Tukey's multiple comparisons test).

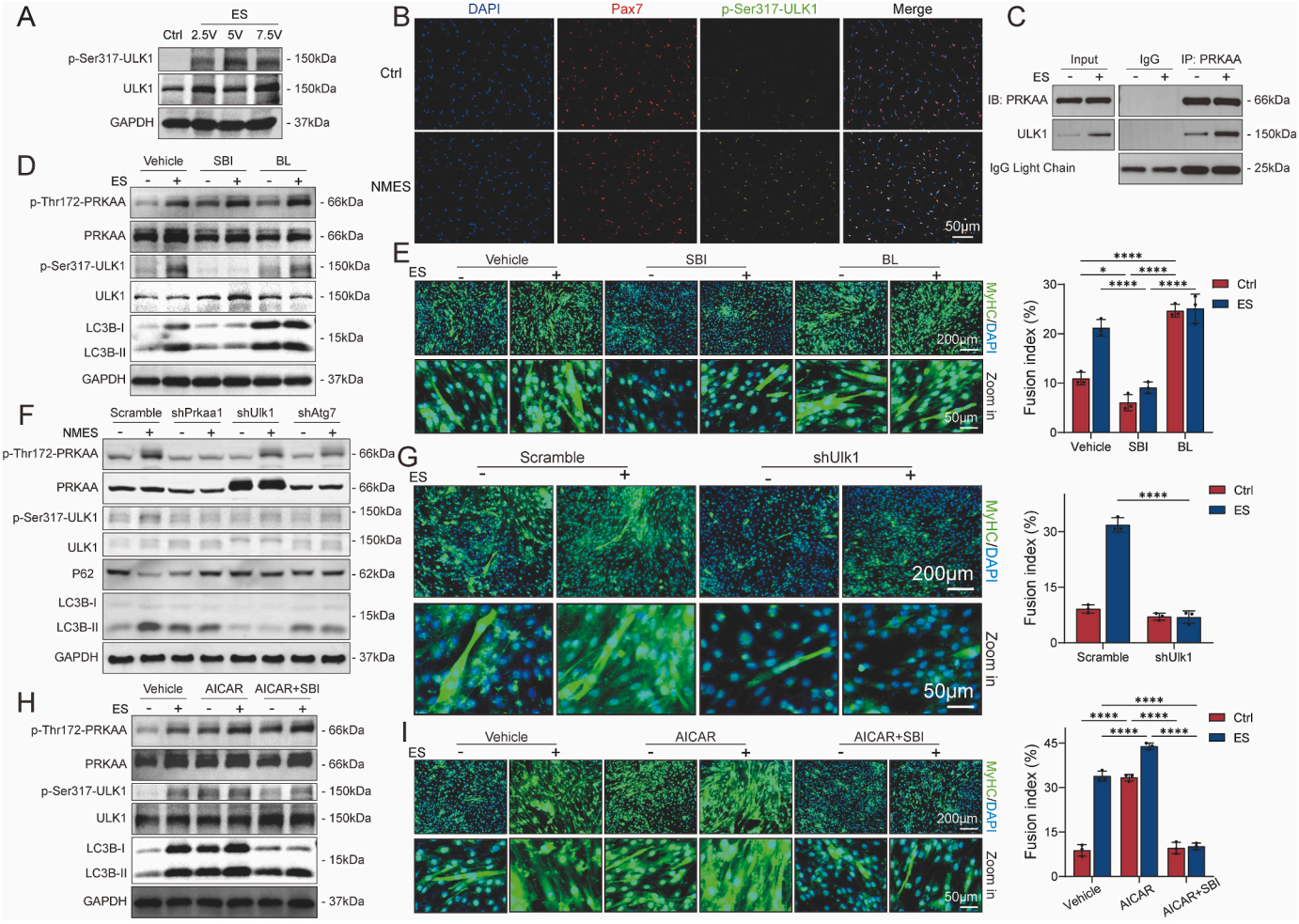

Fig. 7. AMPK phosphorylation of ULK1 was required for ES-induced autophagy and myogenic differentiation. (A) Western Blot analysis of ULK1 activation in MuSCs under control and different voltages for 30min. (B) Immunofluorescence staining for p-Ser317-ULK1, Pax7 and DAPI in muscle with stroke-related sarcopenia from control and NMES-treated rats; scale bar: 50 μm. (C) MuSCs were treated under control and ES conditions (5V treated for 30min). Immunoprecipitation (IP) was performed with PRKAA antibody or pre-immune IgG. Immunoblotting (IB) was carried out to detect PRKAA and ULK1. (D) Western Blot analysis of AMPK-ULK1/autophagic activation in MuSCs treated with ULK1 inhibitor SBI-0206965 (SBI, 1 μM) or agonist BL-918 (15 μM) in control group and ES treatment group. (E) Immunofluorescence staining of MuSCs after myotube differentiation for three days with SBI or BL in control group and ES treatment group; MyHC (green) and DAPI (blue) for myotube; scale bar: 200 μm (magnification zones, scale bar: 50 μm). Quantitative analysis of immunofluorescence intensity for MyHC of the E-panel (three random filed in each group; *$P < 0.05$, ****$P < 0.0001$ by two-way ANOVA, followed by Tukey's multiple comparisons test). (F) Western Blot analysis of AMPK-ULK1/autophagic activation in rats using lentivirus vector-mediated shRNA (LV-Prkaa1shRNA, LV-Atg7shRNA and LV-Ulk1shRNA) in control group and NMES treatment group. (G) Immunofluorescence staining of MuSCs after myotube differentiation for three days infected with scramble or shUlk1 lentivirus in control group and ES treatment group; MyHC (green) and DAPI (blue) for myotube; scale bar: 200 μm (magnification zones, scale bar: 50 μm). Quantitative analysis of immunofluorescence intensity for MyHC of the G-panel (three random filed in each group; ****$P < 0.0001$ by two-way ANOVA, followed by Tukey's multiple comparisons test). (H) Western Blot analysis of AMPK-ULK1-autophagy activation in MuSCs with an PRKAA agonist AICAR (15 μM) or/and ULK1 inhibitor SBI (1 μM) in control group and ES treatment group. (I) Immunofluorescence staining of MuSCs after myotube differentiation for three days with AICAR or/and SBI under control and ES conditions; MyHC (green) and DAPI (blue) for myotube; scale bar: 200 μm (magnification zones, scale bar: 50 μm). Quantitative analysis of immunofluorescence intensity for MyHC of the E-panel (three random filed in each group; ****$P < 0.0001$ by two-way ANOVA, followed by Tukey's multiple comparisons test).

differentiation.

The use of cell therapy for the treatment of stroke has garnered significant interest in the field of regenerative medicine over the past 25 years [65], and involves the utilization of cells or cellular materials with therapeutic effects in animal models of stroke. However, most established therapies focus on repairing neurological damage caused by stroke but continue to face numerous challenges [66]. Moreover, few cell therapy options are available for the treatment of stroke-related sarcopenia. At present, cell therapy strategies using MuSCs have been conducted in small animals [16]. However, MuSCs treatment has only been studied in muscle diseases combined with open trauma [16,17]. Therefore, further research is required to explore the application of direct MuSCs injection *in vivo* for the treatment of muscle degeneration. Moreover, this study employed inhibitors and shRNA techniques in conjunction with ES treatment *in vitro* to emulate NMES treatment *in vivo*, thereby facilitating the identification of its underlying mechanisms. Overall, to the best of our knowledge, this study is the first to demonstrate that NMES treatment can alleviate stroke-related sarcopenia in rats by promoting muscle regeneration via MuSCs autophagy.

AMPK, a critical regulator of growth, reprogramming metabolism, cell polarity, and autophagy, serves as a multifunctional factor in various pathophysiological conditions [32–34]. Previous studies have shown that *in situ* ES of muscles increases AMPK phosphorylation and activity in animal models [37]. PRKAA also stimulates autophagy via mTOR and ULK1 [35,36]. In addition to its role in regulating cell death, autophagy also plays a crucial role in muscle regeneration and has been shown to influence the fate of MuSCs [67]. Some studies have explored the effects of autophagy on muscle differentiation and regeneration and have, ultimately, suggested that autophagy promotes myogenic differentiation and regeneration [68–70]. Currently, we revealed that ES treatment activates PRKAA during myogenic differentiation and induces autophagy through ULK1, rather than mTOR. Specifically, we observed enhanced Ser317 phosphorylation of ULK1 following ES treatment. This PRKAA-dependent phosphorylation of Ser317 has been linked to an increase in ULK1 activity [35,36,71]. However, no significant alterations in mTOR phosphorylation at Ser2448 were observed following ES treatment (Fig. S6A), suggesting that mTOR does not contribute to ES-induced autophagy. Consistently, the phosphorylation level of ULK1 at Ser757, regulated by mTOR and associated with reduced ULK1 activity, was not significantly altered following ES treatment (Fig. S6B). Additionally, co-immunoprecipitation results revealed that AMPK and ULK1 interact during ES treatment. By using a ULK1 inhibitor, shRNA, and agonist, we demonstrated that AMPK-ULK1 is essential for the initiation of ES-induced autophagy and myogenic differentiation in MuSCs.

Finally, we concluded that NMES treatment could restore muscle function, increase muscle mass and promote muscle regeneration in stroke-related sarcopenia by activating MuSCs autophagy via AMPK-ULK1 autophagy axis. In addition, our findings demonstrated that NMES could accelerate muscle function repair process and significantly improve myogenic activity and muscle regeneration in stroke-related sarcopenia rats. Moreover, we utilized ES treatment on primary rat MuSCs *in vitro* and investigated the underlying mechanisms. indicating that ES treatment promoted muscle regeneration. Furthermore, after interfering with inhibitors and shRNA, results showed that ES-associated muscle differentiation occur via MuSCs autophagy, revealing that ES treatment faithfully mimics the myogenic activity and muscle regeneration *in vitro*. Additionally, we found that the activation of AMPK-ULK-autophagy by NMES treatment was verified *in vivo*. These findings revealed that NMES treatment significantly restores muscle function, promotes muscle regeneration, and increases muscle mass *in vivo*.

5. Conclusion

The present results provided insight into the pathological mechanism of NMES treatment alleviating stroke-related sarcopenia. The underlying mechanisms potentially provided novel therapeutic strategy for clinical treatment. NMES combined with MuSCs treatment can improve patient prognosis and quality of survival in the future. However, the *in vivo* mechanism was not confirmed by using genetic models due to poor development of Cre-loxP system in rats. Disputation still remains, considering that primary MuSCs cultured *in vitro* are markedly different from *in vivo* and that using ES-induced myogenic differentiation to dissect biology of NMES-induced muscle regeneration may result in discrepancies. Our experimental design utilizing primary MuSCs cultured *in vitro* instead of use of genetic models for mechanistic investigations did not compromise the accuracy of our conclusions for the following reasons. On the one hand, we observed that NMES treatment activated key proteins on the autophagy axis *in vivo*. On the other hand, we used shRNA technique to specifically knock down each gene in primary MuSCs *in vitro* and reproduce phenotypes achieved by ES treatment and or inhibitors. These complementary approaches conclusively establish that NMES intervention ameliorates stroke-related sarcopenia through AMPK-ULK1-autophagy axis-mediated enhancement of myogenic differentiation.

Declaration of competing interest

The authors declare no competing financial interest.

Data availability

Data will be made available on request.

Ethics approval and consent to participate

All animal procedures were performed in accordance with the protocols approved by the Fudan University Institutional Animal Care and Use Committee (2023-044).

CRediT authorship contribution statement

Conceptualization, TF.F., J.Z., XD.X.; Methodology, L.H., MX.B., WS.C., LY.Q., N.W. and GJ.H.; Investigation, XD.X., GK.M., YX.Z., HL.Y. and C.Z.; Visualization, LY.Q., WC.L. and XD.X.; Supervision, TF.F., SY.L. and J.Z.; Funding Acquisition, TF.F., SY.L. and J.Z.; Writing—original draft, XD.X.; Writing—review & editing: XD.X., TF.F., J.Z., SY.L., WC.L. and L.H.

Declaration of generative AI and AI-assisted technologies in the writing process

The authors completed this manuscript without the use of generative AI and AI-assisted technologies in the writing process.

Funding

This work was supported by the Shanghai Sailing Program (Grant number 21YF1406700, granted to Tengfei Fu), the National Natural Science Foundation of China (Grant number 82202790, granted to Tengfei Fu), the National Science and Natural Science Foundation (Grant number 81870965, granted to Jian Zhang), Jiangsu Funding Program for Excellent Postdoctoral Talent (Grant number 2024ZB491, granted to Shunyi Lu), China Postdoctoral Science Foundation (Grant number 2024M752333, granted to Shunyi Lu), the Shanghai Science and Technology Commission Fund (Grant number S2019-038, granted to Jian Zhang), the Fundamental Research Funds of Zhongshan Hospital, Fudan University (Grant number 2023ZSCX31, granted to Jian Zhang).

Acknowledgments

We thank Zhihui Guo for providing advice on the rat model; We also

thank Wei Xu for helping with RNA-seq analysis.

Appendix A. Supplementary data

Supplementary data to this article can be found online at https://doi.org/10.1016/j.jot.2025.03.021.

Abbreviations

NMES	Neuromuscular electrical stimulation
ES	Electrical stimulation
pMCAO	Permanent middle cerebral artery occlusion
MuSCs	Skeletal muscle satellite cells
AMPK	Adenosine 5′-monophosphate-activated protein kinase
ULK1	Unc-51 like autophagy activating kinase 1
CMAP	Compound muscle action potentials
RH/LH	Right hind/Left hind
DEGs	Differentially expressed genes
KEGG	Kyoto Encyclopedia of Genes and Genomes

References

[1] Graeme J. Hankey. Stroke. Lancet 2017;389:641–54. https://doi.org/10.1016/S0140-6736(16)30962-X.

[2] Wen-Jun Tu, Wang Long-De, Yan Feng, Peng Bin, Yang Hua, Liu Ming, et al. China stroke surveillance report 2021. Mil Med Res 2023;10:33. https://doi.org/10.1186/s40779-023-00463-x.

[3] Ryan Alice S, Ivey Frederick M, Serra Monica C, Hartstein Joseph, Hafer-Macko Charlene E. Sarcopenia and physical function in middle-aged and older stroke survivors. Arch Phys Med Rehabil 2017;98:495–9. https://doi.org/10.1016/j.apmr.2016.07.015.

[4] Li Wei, Yue Tao, Liu Yanming. New understanding of the pathogenesis and treatment of stroke-related sarcopenia. Biomed Pharmacother 2020;131:110721. https://doi.org/10.1016/j.biopha.2020.110721.

[5] Scherbakov Nadja, Sandek Anja, Doehner Wolfram. Stroke-related sarcopenia: specific characteristics. J Am Med Dir Assoc 2015;16:272–6. https://doi.org/10.1016/j.jamda.2014.12.007.

[6] Chargé Sophie BP, Rudnicki Michael A. Cellular and molecular regulation of muscle regeneration. Physiol Rev 2004;84:209–38. https://doi.org/10.1152/physrev.00019.2003.

[7] Rozo Michelle, Li Liangji, Fan Chen-Ming. Targeting β1-integrin signaling enhances regeneration in aged and dystrophic muscle in mice. Nat Med 2016;22:889–96. https://doi.org/10.1038/nm.4116.

[8] Forcina Laura, Miano Carmen, Musarò Antonio. The physiopathologic interplay between stem cells and tissue niche in muscle regeneration and the role of IL-6 on muscle homeostasis and diseases. Cytokine Growth Factor Rev 2018;41:1–9. https://doi.org/10.1016/j.cytogfr.2018.05.001.

[9] Almada Albert E, Wagers Amy J. Molecular circuitry of stem cell fate in skeletal muscle regeneration, ageing and disease. Nat Rev Mol Cell Biol 2016;17:267–79. https://doi.org/10.1038/nrm.2016.7.

[10] Tamaki Tetsuro. Biomedical applications of muscle-derived stem cells: from bench to bedside. Expet Opin Biol Ther 2020;20:1361–71. https://doi.org/10.1080/14712598.2020.1793953.

[11] Li Hongshuai, Lu Aiping, Tang Ying, Beckman Sarah, Nakayama Naoki, Poddar Minakshi, et al. The superior regenerative potential of muscle-derived stem cells for articular cartilage repair is attributed to high cell survival and chondrogenic potential. Mol Ther Methods Clin Dev 2016;3:16065. https://doi.org/10.1038/mtm.2016.65.

[12] Saverio Tedesco Francesco, Dellavalle Arianna, Diaz-Manera Jordi, Messina Graziella, Cossu Giulio. Repairing skeletal muscle: regenerative potential of skeletal muscle stem cells. J Clin Investig 2010;120:11–9. https://doi.org/10.1172/JCI40373.

[13] Cai Zijun, Liu Di, Yang Yuntao, Xie Wenqing, He Miao, Yu Dengjie, et al. The role and therapeutic potential of stem cells in skeletal muscle in sarcopenia. Stem Cell Res Ther 2022;13:28. https://doi.org/10.1186/s13287-022-02706-5.

[14] Kuang Shihuan, Rudnicki Michael A. The emerging biology of satellite cells and their therapeutic potential. Trends Mol Med 2008;14:82–91. https://doi.org/10.1016/j.molmed.2007.12.004.

[15] Sousa-Victor Pedro, García-Prat Laura, Muñoz-Cánoves Pura. Control of satellite cell function in muscle regeneration and its disruption in ageing. Nat Rev Mol Cell Biol 2022;23:204–26. https://doi.org/10.1038/s41580-021-00421-2.

[16] Han Woojin M, Anderson Shannon E, Mohiuddin Mahir, Barros Daniela, Nakhai Shadi A, Shin Eunjung, et al. Synthetic matrix enhances transplanted satellite cell engraftment in dystrophic and aged skeletal muscle with comorbid trauma. Sci Adv 2018;4:eaar4008. https://doi.org/10.1126/sciadv.aar4008.

[17] Lu S, Yang Y, Song Z, Cao J, Han Z, Chen L, et al. Dual functional nanoplatforms potentiate osteosarcoma immunotherapy via microenvironment modulation. Natl Sci Rev 2025;12:nwaf002. https://doi.org/10.1093/nsr/nwaf002.

[18] Kaneshige Akihiro, Kaji Takayuki, Zhang Lidan, Saito Hayato, Nakamura Ayasa, Kurosawa Tamaki, et al. Relayed signaling between mesenchymal progenitors and muscle stem cells ensures adaptive stem cell response to increased mechanical load. Cell Stem Cell 2022;29:265–280.e6. https://doi.org/10.1016/j.stem.2021.11.003.

[19] Li Weijun, Zhu Zhenhong, He Kai, Ma Xiaoyu, Pignolo Robert J, Sieck Gary C, et al. Primary cilia in satellite cells are the mechanical sensors for muscle hypertrophy. Proc Natl Acad Sci 2022;119:e2103615119. https://doi.org/10.1073/pnas.2103615119.

[20] Adams Volker. Electromyostimulation to fight atrophy and to build muscle: facts and numbers. J Cachexia Sarcopenia Muscle 2018;9:631–4. https://doi.org/10.1002/jcsm.12332.

[21] Qian Li, Huang Yu, Ian Spencer C, Foley Amy, Vedantham Vasanth, Liu Lei, et al. In vivo reprogramming of murine cardiac fibroblasts into induced cardiomyocytes. Nature 2012;485:593–8. https://doi.org/10.1038/nature11044.

[22] Oh Byeongtaek, Wu Yu-Wei, Swaminathan Vishal, Lam Vivek, Ding Jun, George Paul M. Modulating the electrical and mechanical microenvironment to guide neuronal stem cell differentiation. Adv Sci 2021;8:2002112. https://doi.org/10.1002/advs.202002112.

[23] Doucet Barbara M, Lam Amy, Griffin Lisa. Neuromuscular electrical stimulation for skeletal muscle function. Yale J Biol Med 2012;85:201–15.

[24] Rabelo Michelle, Juca Renata Viana Brigido de Moura, Lima Lidiane Andrea Oliveira, Resende-Martins Henrique, Bo Antonio Padilha Lanari, Fattal Charles, et al. Overview of FES-assisted cycling approaches and their benefits on functional rehabilitation and muscle atrophy. In: Xiao J, editor. Muscle atrophy, vol. 1088. Singapore: Springer-Verlag Singapore Pte Ltd; 2018. p. 561–83. https://doi.org/10.1007/978-981-13-1435-3_26.

[25] Crema Andrea, Bassolino Michela, Guanziroli Eleonora, Colombo Maria, Blanke Olaf, Serino Andrea, et al. Neuromuscular electrical stimulation restores upper limb sensory-motor functions and body representations in chronic stroke survivors. Med N Y N 2022;3:58–74.e10. https://doi.org/10.1016/j.medj.2021.12.001.

[26] Blazevich Anthony J, Collins David F, Millet Guillaume Y, Vaz Marco A, Maffiuletti Nicola A. Enhancing adaptations to neuromuscular electrical stimulation training interventions. Exerc Sport Sci Rev 2021;49:244–52. https://doi.org/10.1249/JES.0000000000000264.

[27] Dirks ML, Wall BT, Snijders T, Ottenbros CLP, Verdijk LB, van Loon LJC. Neuromuscular electrical stimulation prevents muscle disuse atrophy during leg immobilization in humans. Acta Physiol 2014;210:628–41. https://doi.org/10.1111/apha.12200.

[28] Putman Charles T, Sultan Karim R, Wassmer Thomas, Bamford Jeremy A, Škorjanc Dejan, Pette Dirk. Fiber-type transitions and satellite cell activation in low-frequency-stimulated muscles of young and aging rats. J Gerontol Ser A 2001;56:B510–9. https://doi.org/10.1093/gerona/56.12.B510.

[29] Mizushima Noboru. A brief history of autophagy from cell biology to physiology and disease. Nat Cell Biol 2018;20:521–7. https://doi.org/10.1038/s41556-018-0092-5.

[30] Rubinsztein David C, Codogno Patrice, Beth Levine. Autophagy modulation as a potential therapeutic target for diverse diseases. Nat Rev Drug Discov 2012;11:709–30. https://doi.org/10.1038/nrd3802.

[31] Bento Carla F, Renna Maurizio, Ghislat Ghita, Puri Claudia, Ashkenazi Avraham, Vicinanza Mariella, et al. Mammalian autophagy: how does it work? Annu Rev Biochem 2016;85:685–713. https://doi.org/10.1146/annurev-biochem-060815-014556.

[32] Kim Joungmok, Yang Goowon, Kim Yeji, Kim Jin, Ha Joohun. AMPK activators: mechanisms of action and physiological activities. Exp Mol Med 2016;48:e224. https://doi.org/10.1038/emm.2016.16.

[33] Oakhill Jonathan S, Steel Rohan, Chen Zhi-Ping, Scott John W, Ling Naomi, Tam Shanna, et al. AMPK is a direct adenylate charge-regulated protein kinase. Science 2011;332:1433–5. https://doi.org/10.1126/science.1200094.

[34] Mihaylova Maria M, Shaw Reuben J. The AMPK signalling pathway coordinates cell growth, autophagy and metabolism. Nat Cell Biol 2011;13:1016–23. https://doi.org/10.1038/ncb2329.

[35] Kim Joungmok, Kundu Mondira, Viollet Benoit, Guan Kun-Liang. AMPK and mTOR regulate autophagy through direct phosphorylation of Ulk1. Nat Cell Biol 2011;13:132–41. https://doi.org/10.1038/ncb2152.

[36] Egan Dan, Kim Joungmok, Shaw Reuben J, Guan Kun-Liang. The autophagy initiating kinase ULK1 is regulated via opposing phosphorylation by AMPK and mTOR. Autophagy 2011;7:643–4. https://doi.org/10.4161/auto.7.6.15123.

[37] Thomson DM, Porter BB, Tall JH, Kim H-J, Barrow JR, Winder WW. Skeletal muscle and heart LKB1 deficiency causes decreased voluntary running and reduced muscle mitochondrial marker enzyme expression in mice. Am J Physiol Endocrinol Metab 2007;292:E196–202. https://doi.org/10.1152/ajpendo.00366.2006.

[38] Longa EZ, Weinstein PR, Carlson S, Cummins R. Reversible middle cerebral artery occlusion without craniectomy in rats. Stroke 1989;20:84–91. https://doi.org/10.1161/01.str.20.1.84.

[39] Bai Shanshan, Lu Xuan, Qi Pan, Wang Bin, Kin Pong U, Yang Yongkang, et al. Cranial bone transport promotes angiogenesis, neurogenesis, and modulates meningeal lymphatic function in middle cerebral artery occlusion rats. Stroke 2022;53:1373–85. https://doi.org/10.1161/STROKEAHA.121.037912.

[40] Bärmann J, Walter HL, Pikhovych A, Endepols H, Fink GR, Rueger MA, et al. An analysis of the CatWalk XT and a composite score to assess neurofunctional deficits after photothrombosis in mice. Neurosci Lett 2021;751:135811. https://doi.org/10.1016/j.neulet.2021.135811.

[41] Pawletko Katarzyna, Jędrzejowska-Szypułka Halina, Bogus Katarzyna, Pascale Alessia, Fahmideh Foroogh, Marchesi Nicoletta, et al. After ischemic

stroke, minocycline promotes a protective response in neurons via the RNA-binding protein HuR, with a positive impact on motor performance. Int J Mol Sci 2023;24:9446. https://doi.org/10.3390/ijms24119446.
[42] Moyle Louise A, Isolation Peter S Zammit. Culture and immunostaining of skeletal muscle fibres to study myogenic progression in satellite cells. In: Kioussi Chrissa, editor. Stem cells tissue repair methods protoc. New York, NY: Springer; 2014. p. 63–78. https://doi.org/10.1007/978-1-4939-1435-7_6.
[43] Kim Daehwan, Paggi Joseph M, Park Chanhee, Bennett Christopher, Salzberg Steven L. Graph-based genome alignment and genotyping with HISAT2 and HISAT-genotype. Nat Biotechnol 2019;37:907–15. https://doi.org/10.1038/s41587-019-0201-4.
[44] Li Heng, Handsaker Bob, Wysoker Alec, Fennell Tim, Ruan Jue, Homer Nils, et al. The sequence alignment/map format and SAMtools. Bioinforma Oxf Engl 2009;25:2078–9. https://doi.org/10.1093/bioinformatics/btp352.
[45] Love Michael I, Huber Wolfgang, Anders Simon. Moderated estimation of fold change and dispersion for RNA-seq data with DESeq2. Genome Biol 2014;15:550. https://doi.org/10.1186/s13059-014-0550-8.
[46] Kolde Raivo. raivokolde/pheatmap. 2025.
[47] Yu Guangchuang, Wang Li-Gen, Han Yanyan, He Qing-Yu. clusterProfiler: an R package for comparing biological themes among gene clusters. OMICS A J Integr Biol 2012;16:284–7. https://doi.org/10.1089/omi.2011.0118.
[48] Walter Wencke, Sánchez-Cabo Fátima, Ricote Mercedes. GOplot: an R package for visually combining expression data with functional analysis. Bioinforma Oxf Engl 2015;31:2912–4. https://doi.org/10.1093/bioinformatics/btv300.
[49] Klionsky Daniel J, Abdel-Aziz Amal Kamal, Abdelfatah Sara, Abdellatif Mahmoud, Abdoli Asghar, Abel Steffen, et al. Guidelines for the use and interpretation of assays for monitoring autophagy (4th edition)1. Autophagy 2021;17:1–382. https://doi.org/10.1080/15548627.2020.1797280.
[50] Schmidt Manuel, Schüler Svenja C, Hüttner Sören S, von Eyss Björn, von Maltzahn Julia. Adult stem cells at work: regenerating skeletal muscle. Cell Mol Life Sci CMLS 2019;76:2559–70. https://doi.org/10.1007/s00018-019-03093-6.
[51] Bujak Adam L, Crane Justin D, Lally James S, Ford Rebecca J, Kang Sally J, Rebalka Irena A, et al. AMPK activation of muscle autophagy prevents fasting-induced hypoglycemia and myopathy during aging. Cell Metab 2015;21:883–90. https://doi.org/10.1016/j.cmet.2015.05.016.
[52] Nakatogawa Hitoshi, Suzuki Kuninori, Kamada Yoshiaki, Ohsumi Yoshinori. Dynamics and diversity in autophagy mechanisms: lessons from yeast. Nat Rev Mol Cell Biol 2009;10:458–67. https://doi.org/10.1038/nrm2708.
[53] Watson BD, Dietrich WD, Busto R, Wachtel MS, Ginsberg MD. Induction of reproducible brain infarction by photochemically initiated thrombosis. Ann Neurol 1985;17:497–504. https://doi.org/10.1002/ana.410170513.
[54] Bauer Juergen, Morley John E, Schols Annemie MW J, Ferrucci Luigi, Cruz-Jentoft Alfonso J, Dent Elsa, et al. Sarcopenia: a time for action. An SCWD position paper. J Cachexia Sarcopenia Muscle 2019;10:956–61. https://doi.org/10.1002/jcsm.12483.
[55] Bonaldo Paolo, Sandri Marco. Cellular and molecular mechanisms of muscle atrophy. Dis Model Mech 2013;6:25–39. https://doi.org/10.1242/dmm.010389.
[56] Vainshtein Anna, Grumati Paolo, Sandri Marco, Bonaldo Paolo. Skeletal muscle, autophagy, and physical activity: the ménage à trois of metabolic regulation in health and disease. J Mol Med Berl Ger 2014;92:127–37. https://doi.org/10.1007/s00109-013-1096-z.
[57] Méndez-López Iago, Sancho-Bielsa Francisco J, Engel Tobias, García Antonio G, Padín Juan Fernando. Progressive mitochondrial SOD1G93A accumulation causes severe structural, metabolic and functional aberrations through OPA1 down-regulation in a mouse model of amyotrophic lateral sclerosis. Int J Mol Sci 2021;22:8194. https://doi.org/10.3390/ijms22158194.
[58] von Maltzahn Julia, Bentzinger C Florian, Rudnicki Michael A. Characteristics of satellite cells and multipotent adult stem cells in the skeletal muscle. In: Hayat MA, editor. Stem cells cancer stem cells. Ther. Appl. Dis. Inj., vol. 12. Dordrecht: Springer Netherlands; 2014. p. 63–73. https://doi.org/10.1007/978-94-017-8032-2_6.
[59] Florian Bentzinger C, Xin Wang Yu, Rudnicki Michael A. Building muscle: molecular regulation of myogenesis. Cold Spring Harb Perspect Biol 2012;4:a008342. https://doi.org/10.1101/cshperspect.a008342.
[60] Singh Kulwant, Jeffrey Dilworth F. Differential modulation of cell cycle progression distinguishes members of the myogenic regulatory factor family of transcription factors. FEBS J 2013;280:3991–4003. https://doi.org/10.1111/febs.12188.
[61] Soleimani Vahab D, Punch Vincent G, Kawabe Yoh-ichi, Jones Andrew E, Palidwor Gareth A, Porter Christopher J, et al. Transcriptional dominance of Pax7 in adult myogenesis is due to high-affinity recognition of homeodomain motifs. Dev Cell 2012;22:1208–20. https://doi.org/10.1016/j.devcel.2012.03.014.
[62] Manuel Hernández-Hernández J, García-González Estela G, Brun Caroline E, Rudnicki Michael A. The myogenic regulatory factors, determinants of muscle development, cell identity and regeneration. Semin Cell Dev Biol 2017;72:10–8. https://doi.org/10.1016/j.semcdb.2017.11.010.
[63] Stark Danny A, Karvas Rowan M, Siegel Ashley L, Cornelison DDW. Eph/ephrin interactions modulate muscle satellite cell motility and patterning. Dev Camb Engl 2011;138:5279–89. https://doi.org/10.1242/dev.068411.
[64] Florian Bentzinger C, von Maltzahn Julia, Dumont Nicolas A, Stark Danny A, Wang Yu Xin, Nhan Kevin, et al. Wnt7a stimulates myogenic stem cell motility and engraftment resulting in improved muscle strength. J Cell Biol 2014;205:97–111. https://doi.org/10.1083/jcb.201310035.
[65] Savitz Sean I. Developing cellular therapies for stroke. Stroke 2015;46:2026–31. https://doi.org/10.1161/STROKEAHA.115.007149.
[66] Misra Vivek, Hicks William J, Vahidy Farhaan, Alderman Susan, Savitz Sean I. Recruiting patients with stroke into cell therapy trials. 2016.
[67] Chen Wei, Chen Yushi, Liu Yuxi, Wang Xinxia. Autophagy in muscle regeneration: potential therapies for myopathies. J Cachexia Sarcopenia Muscle 2022;13:1673–85. https://doi.org/10.1002/jcsm.13000.
[68] Call Jarrod A, Wilson Rebecca J, Laker Rhianna C, Zhang Mei, Kundu Mondira, Yan Zhen. Ulk1-mediated autophagy plays an essential role in mitochondrial remodeling and functional regeneration of skeletal muscle. Am J Physiol Cell Physiol 2017;312:C724–32. https://doi.org/10.1152/ajpcell.00348.2016.
[69] Jon Sin, Andres Allen M, Taylor David JR, Weston Thomas, Hiraumi Yoshimi, Stotland Aleksandr, et al. Mitophagy is required for mitochondrial biogenesis and myogenic differentiation of C2C12 myoblasts. Autophagy 2016;12:369–80. https://doi.org/10.1080/15548627.2015.1115172.
[70] McMillan Elliott M, Quadrilatero Joe. Autophagy is required and protects against apoptosis during myoblast differentiation. Biochem J 2014;462:267–77. https://doi.org/10.1042/BJ20140312.
[71] Alers Sebastian, Löffler Antje S, Wesselborg Sebastian, Stork Björn. Role of AMPK-mTOR-Ulk1/2 in the regulation of autophagy: cross talk, shortcuts, and feedbacks. Mol Cell Biol 2012;32:2–11. https://doi.org/10.1128/MCB.06159-11.